

**Assessing the distribution and abundance of seabed minerals from seafloor
photography data in the Central Indian Ocean Basin**

(Running head: Estimation of minerals using seabed photos from CIOB)

RAHUL SHARMA, N.H. KHADGE* and S. JAI SANKAR
National Institute of Oceanography
(Council of Scientific and Industrial Research)
Dona Paula, Goa - 403004, India

Abstract

Distribution characteristics of deep-sea mineral resources such as polymetallic nodules and ferromanganese crusts are often influenced by local seafloor features such as the topographic undulations and sediment thickness. Qualitative as well as semi-quantitative estimation of these resources have been attempted earlier by using seafloor photography data. This study analyzes the distribution of these minerals in relation to their associated seafloor surface features and develops empirical formulae for abundance estimation of a deposit from photography data in conjunction with sounding and sampling data in Central Indian Ocean Basin. Data from >20,000 photos were analyzed and correlated with geological features such as bathymetry, sediment thickness and sediment physical properties. The study showed that nodule populations are negatively correlated with the thickness of the acoustically transparent layer (ATL), which in turn is controlled by the topographic undulations. The variable burial of nodules under the ATL, as indicated by sampling data, leads to underestimation of nodules from photographs. In order to improve the accuracy of such estimations, different constant factors (C factor) have been proposed for use in empirical formulae depending upon the distribution characteristics of the deposits.

*Corresponding author. Email address: khadge@nio.org

1. Introduction

Seabed minerals such as polymetallic or ferromanganese nodules have been reported from the Pacific, Atlantic and the Indian Oceans (Cronan *et al.* 2000). The distribution of these deep-sea mineral deposits are influenced by several factors, such as the associated environment (e.g. lithogenic, biogenic, chemogenic), sediment type (e.g. siliceous, calcareous, and pelagic) and water depth (Frazer and Fisk, 1981; Cronan, 1980). Traditionally, acquisition of seabed samples for analyses has been carried out using devices such as grabs and corers, which are time-consuming. On the other hand, seafloor photography, due to its ability to record large number of pictures in a short time period, has developed as an effective tool for gathering a variety of information (Jung *et al.*, 2001; Edwards *et al.*, 2003) that can be complemented with ground truth data.

There have also been several questions regarding the reliability of the sampling devices for not being successful in collecting the nodules and/or rock/crust outcrops due to their operational limitations vis-à-vis the photographs that are likely to yield more information (UNOET, 1982), as the photography technique provides a visual evidence of the existence of the mineral as well as recording the associated substrates (Fig. 1). Seafloor photographs have been used for semi-quantitative assessment of nodule distribution on the seafloor (Glasby, 1976; Frazer *et al.* 1978; Jung *et al.* 2001); analyzing their relation with different topographic features (Yamazaki and Sharma, 2000); evaluating deep seafloor environments associated with polymetallic nodules (Sharma and Rao, 1992; Shipek, 2009); as well as studying the impact of experimental mining on megafauna (Rodrigues *et al.* 2001; Bluhm *et al.* 2001). Having the ability of recording several thousand photographs in a single run (Fewkes *et al.* 1979; Sharma *et al.* 2010), also make it a technique for fast reconnaissance surveys followed by physical sampling in areas of interest.

Some of the previous studies have attempted to develop methods to quantify nodule coverage from photographic data in limited areas, by using planimeter and point counting techniques (Fewkes *et al.* 1979); measuring morphological features of nodules (Lenoble, 1980); applying coverage and nodule diameter (Handa and Tsurusaki, 1981); as well as employing image processing techniques (Park *et al.* 1997). This study assesses the distribution of nodules and crusts on a basin scale using >20000 images and relating them to the geological features associated with them in the Central Indian Ocean Basin (CIOB) and attempts to develop empirical relationships to estimate the nodule abundance from seafloor photographs.

2. Materials and methods

Seafloor photography data was collected using deep-towed photography system that comprises a tow-body with cameras capable of recording a series of photos at pre-fixed intervals, just above the seafloor; a depressor that stabilizes the tow-body; both of which are connected through a coaxial cable with the deck-unit on the research vessel, from where the system is operated. This study is based on 20,506 seafloor photographs taken with the deep-towed photography system along 5 profiles in the CIOB (Fig. 2) onboard RV AA Sidorenko and processed subsequently using a specially developed image analysis system with ERDAS (Sharma *et al.* 2010).

The coverage of nodules, crusts and sediments on the seafloor as well as the depth and slope angles at the locations of the photographs were plotted using Surfer (8.0) software. Although, the influence of survey lines is seen in the plots (Figs. 3-7) due to the distance between them, it does not alter the interpretation. These were correlated with sediment thickness data from Parasound records from cruises onboard RV Boris Petrov in 2006 and 2008; and with nodule abundance data from freefall grabs from earlier cruises in CIOB, as well as box core samples collected onboard RV Boris Petrov in 2008. The physical properties of the sediments associated with nodules were analyzed as described in Khadge (2005). This study also uses the equation proposed by Handa and Tsurusaki (1981) to work out the constant factors to be used for estimating nodule abundances from photographs in CIOB.

3. Results

a. Distribution of nodules and associated seafloor features

The topographic map (Fig. 3) shows a relatively flat northern area (north of 13°S) and an undulating topography with abyssal hills in the southern area (south of 13°S), water depth ranging from 4975 to 5433 m with a mean of ~5205 m (Table 1).

Nodule coverage, as estimated from the photographs, ranges from 0% to 79% with a mean of 8.95% owing to a high percentile of data being 0% (Table 1). The nodule coverages (Fig. 4) are relatively higher in the southern part of the area (south of 13°S) as compared to the north (north of 13°S).

Crust coverage ranges from 0 to 89% with a very low mean of 0.28% (Table 1) as most photographs (~99%) have no crust outcrops recorded in the photographs. Also most of the crust exposures are in the southern part of the area (south of 13°S) as compared to the north, but owing to their occurrence at very few locations (1%), they cannot be visualized on the map (Fig. 5).

Sediment coverage ranges from 0% to 100% with a high mean of 89.6% due to high percentile data lying between 80-100% (Table 1). Variability in sediment cover, however, is higher in the southern part (south of 13°S), whereas the northern part has a fairly uniform coverage close to 100% (Fig. 6).

Seabed slopes vary from 0° to 76° in the entire area with a mean of 2° (Table 1). Higher slope angles are noticed in the southern part (south of 13°S) which also has more undulating topography as compared to the northern part (Fig. 7).

The above data bring out the following observations:

- i. More undulating topography is to the south of 13° S latitude
- ii. Higher nodule coverages are to the south of 13° S latitude
- iii. More crust exposures are to the south of 13° S latitude
- iv. Variable sediment cover is to the south of 13° S latitude
- v. Higher slope angles are to the south of 13° S latitude

These observations indicate that the higher nodule coverages (and also crust exposures) are associated with undulating topography, whereas the relatively flat seafloor hosts higher sediment cover. The undulating topography seems to be responsible for sediment particles being washed off into the intervening valleys, thus leading to exposure of nodules and crusts for their growth; as well as the rock outcrops, fragmentation of which due to physical processes, provides nuclei for nodule formation. Conversely, the flat topography hosts a uniform layer of sediment leading to burial of nodules as well as rock outcrops, hence restricting the growth of ferromanganese oxides on them, as well as acting as a blanket for their exposure. The 'seed' hypothesis by Horn *et al.* (1973) in the Pacific Ocean and the studies on association of higher nodule occurrences with undulating topography in the Indian Ocean (Sharma and Kodagali, 1993), also support such a relationship between nodule distribution and topography as well as sediment cover; that could also be responsible for the morphology and composition of the nodules (Mukhopadhyay and Nath, 1988).

Although many (65%) of the photographs in the area do not show nodules exposed on the seafloor (Sharma *et al.* 2010), their existence is confirmed from 335 freefall grab samples collected in the area, wherein the mean nodule abundances in most (9 out of 12) blocks of 0.5° x 0.5° are ~5 to 8 kg m⁻² (Fig. 8) implying that nodules at many locations in CIOB are buried in the top 20-25 cm to which the freefall grabs can penetrate. Hence, the role of sediment cover achieves more significance

in non-exposure (or burial) of nodules. The distribution of this top sediment layer or acoustically transparent layer in turn is controlled by the topographic undulations, as seen from the next section.

b. Relation of nodule distribution with topography and sediment cover

Analysis of thickness of acoustically transparent layer (ATL) from Parasound data in different topographic domains shows that it can vary from a few meters to several tens of meters as seen at 2 locations in the area (Fig. 9a and 9b). The figures clearly show a change in density of this top fluffy layer with respect to the overlying water column and the underlying compact sediment layer. Although the ATL thickness at these locations is different, the sediments have similar physical properties (Table 2), indicating that the thickness is influenced by factors other than the sediment properties. Analysis of this layer from Parasound records at several locations shows that ATL thickness at many locations (50%) on the peaks of abyssal hills is small (<10m), whereas in the valleys majority of the locations (>60%) have a higher thickness (30-60m), and the slopes have a variable thickness (Fig. 10), indicating that the thickness of ATL is influenced by topographic undulations.

The nodule samples collected along the Parasound tracks (Table 3) show that the nodule abundances have a negative correlation with the thickness of the sediment layer (Fig. 11). Although this correlation is weak ($r = -0.473$), it does indicate the role of sediment cover in nodule distribution, as this 'fluffy' layer is responsible for partial or complete burial of nodules causing problems in estimating nodule populations from photography data (Fewkes *et al.* 1979; Felix, 1980; Sharma, 1989). This calls for the use of a 'correction' factor (or a constant factor) for accounting the buried nodules which is attempted in the following section.

c. Estimation of abundance using different constant factors for nodule coverage

Some of the previous studies conducted in the Pacific Ocean (Felix, 1980; Handa and Tsurusaki, 1981) have attempted to develop empirical formulae using grab and photographic data from the same locations that can be applied for estimating nodule abundance from photography data alone, by using a constant factor along with nodule diameter and coverage as inputs from the photographs. Owing to different geological settings, however, it is necessary to develop different formulae not only for each area, but also for different nodule distribution characteristics. In this study, grab sample data from fourteen locations corresponding to the photographs on deep-tow profiles were evaluated in order to develop a method for estimating nodule abundance from seafloor photographs for CIOB (Table 4). Out of these, seafloor photographs at 7 locations did not have any nodules exposed on the seafloor (0% coverage), whereas in the remaining 7 locations, nodule coverage was variable (5-56 %).

Based on available data from grabs and photographs, constant factor (C factor) was worked out as follows:

$$\text{Abundance} = \text{C factor} \times \text{Dia} \times \text{Cov} / 100 \quad (1)$$

$$\text{Hence, C factor} = \text{Abundance} \times 100 / \text{Dia} \times \text{Cov} \quad (2)$$

Where, C factor is the constant factor to be applied

Abundance is in kg m^{-2}

Dia is nodule diameter in cm

Cov is nodule coverage in %

For this study, average nodule diameter is taken as 2 cm, which is the lower value of the dominant size class of 2-4 cm reported in previous studies from the area (Valsangkar and Khadge, 1989; Sharma, 1998; Vineesh *et al.* 2009). Owing to the fact that nodule distribution is not uniform in the nodule fields, the data was classified in two categories: case 1- where seafloor photographs had nodules exposed on the seafloor (representing continuous distribution of nodules); and, case 2 - all locations, including those where seafloor photographs had no nodule coverage (representing patchy or discontinuous distribution of nodules), for working out the C factor, as follows:

For case 1: only the locations with nodule coverage >0% and Dia =2 cm:

$$\Sigma \text{Cov} / \text{no. of locations} = 250/7 = \text{Avg. Cov.} = 35.7\%, \text{ and similarly}$$

$$\Sigma \text{Abundance} / \text{no. of locations} = 74.51/7 = \text{Avg. Abundance} = 10.64 \text{ kg m}^{-2}$$

$$\text{C factor} = 10.64 \times 100 / 2 \times 35.7 = 14.90 \quad (3)$$

For case 2: all locations including nodule coverage =0% and Dia =2 cm:

$$\Sigma \text{Cov} / \text{no. of locations} = 250/14 = \text{Avg. Cov.} = 17.8 \%, \text{ and similarly}$$

$$\Sigma \text{Abundance} / \text{no. of locations} = 93.31/14 = \text{Avg. Abundance} = 6.665 \text{ kg m}^{-2}$$

$$\text{C factor} = 6.665 \times 100 / 2 \times 17.8 = 18.72 \quad (4)$$

Having worked out the constant factors for estimating nodule abundance from seafloor photographs, there are 2 possibilities for using them:

- i. Use the C factor (i.e. 14.90) worked out for locations where nodules are recorded/recovered both in photos and grabs,

ii. Use the C factor (i.e. 18.72) worked out for locations where nodules were not recorded in photos but recovered in grabs.

The choice of the C factor to be used will depend on the nodule distribution characteristics in the area of application, i.e. if there are patches of no exposed nodules within nodule fields, then the C factor of 18.72 may be used, and if all photos show exposed nodules, then C factor of 14.90 may be used for estimation of nodule abundance. However, for a conservative estimate use of C factor of 14.90 may be more advisable in order to avoid over estimation. In either case, nodule coverage of 13.35% (for C factor of 18.72) and 16.78% (for C factor of 14.90) are the estimated cutoffs for obtaining the required 5 kg m^{-2} abundance, as follows:

i. $5 \text{ kg m}^{-2} = 18.72 \times 2 \text{ cm} \times \text{Cov} / 100$, hence $\text{Cov} = 5 \times 100 / 18.72 \times 2 = 13.35 \%$

ii. $5 \text{ kg m}^{-2} = 14.90 \times 2 \text{ cm} \times \text{Cov} / 100$, hence $\text{Cov} = 5 \times 100 / 14.90 \times 2 = 16.78 \%$

The ratio between the abundances calculated for different nodule coverages (10-100 %) is 0.79:1.00 (Table 5). Here, it is significant to note that nodule abundance calculated at 20% coverage in either case exceeds the cutoff abundance value of 5 kg m^{-2} as recommended by UNOET (1982) for mining. Although, as seen from distribution of nodule coverage (Sharma et al, 2010) in the area, most locations (>80 %) have nodule coverage ranging up to 20 %. Low coverage values of nodules need not be a cause for concern from the point of view of the resource, as buried nodules are not accounted for in photography data. It should also be noted that the nodule diameter considered for these estimations is only 2 cm, and it is likely to have higher average nodule diameters in many locations, leading to higher nodule abundances.

4. Discussion

The distribution characteristics of nodules and crusts are mainly controlled by topographic undulations on the seafloor characterized by seamounts or abyssal hills, their slopes, and the intervening plains and valleys (Sharma and Kodagali, 1993). Whereas, the peaks of seamounts and abyssal hills are favoured locations for rock outcrops and crust exposures; the availability of rock fragments as nuclei and thin sediment cover, enables accretion of more abundant nodules along the slopes and flanks; whereas partial to complete burial of nodules under the sediments is common in the plains and valleys (Iyer and Sharma, 1990). Co-existence of pumice and nodule fields in the CIOB (Iyer and Sudhakar, 1993) and the results of this study are in confirmation of the 'seed' hypothesis of Horn *et al.* (1973).

Several techniques have been used for collecting data on distribution characteristics of deep seafloor minerals such as polymetallic nodules and the associated features, that include direct

methods (mechanical and geochemical) and indirect methods (visual and geophysical), each one having certain advantages and disadvantages in usage and applications (Cronan, 1980; Kunzendorf, 1986; UNOET, 1982). Techniques have also been developed for indirect measurements using multi-beam backscatter data which can provide semi-quantitative coverage estimates of nodules (DeMoustier, 1985; Chakraborty *et al.* 1996). Development of photographic techniques, however, as a faster and more efficient tool has caught the attention of several researchers owing to its capability to capture the minerals in their in situ environmental setup (Glasby, 1976; Fewkes *et al.* 1979; Sharma, 1993; Shipek, 2009).

Whereas, the photographic technique appears to be a reliable one for the exposed nodules (UNOET, 1982), the fact that the nodules may be partly or fully buried, poses a problem in accurate measurement of nodule populations. Although most of the buried nodules occur in the top 30 cm of sediment cover (Felix, 1980; Sharma, 1989), occasionally they are also known to occur down to 6m (Pattan and Parthiban, 2007). The collection of nodules in grabs and corers, however, where many of them have not been recorded on the photographs (Mero, 1962; Felix, 1980; Sharma, 1989), confirm the occurrence of nodules buried under top sediment layers that need to be accounted for resource estimation. Such estimations become more complex due to the non-uniform distribution of nodules on the seafloor, but ‘if the population is defined as the total seafloor area photographed during a bottom camera traverse, then the accuracy is much greater’ (Fewkes *et al.* 1979). Moreover, the smaller the nodules, the higher the chances of them remaining buried (UNOET, 1982; Sharma, 1989).

In order to overcome the problem of burial of nodules in estimating the third dimension and, hence, in resource evaluation, appropriate corrections need to be worked out along with ground truth data on localized nodule distribution patterns and the sounding data for associated seafloor conditions. These corrections when applied with the empirical formulae at different locations and a detailed analyses of distribution characteristics of nodules, crusts and sediments in relation to seabed topography and slopes, helps in mapping of these deposits. This provides useful inputs for selection of mine-site and designing of mining systems (Yamazaki and Sharma, 2000).

5. Conclusion

Quantitative estimation of nodules from photographs requires special care as visual estimates tend to be subjective, whereas those made using electronic methods are limited by the analyzer’s ability to discriminate between nodules and sediments in photographs (Fewkes *et al.* 1979). Although the photographs cover a much larger area than other sampling devices, the thickness of nodules cannot

be estimated (Lenoble, 1980). Development of image processing technique (Park *et al.* 1978), enhanced by user-interfaced image analysis to improve the accuracy of photography data (Sharma *et al.* 2010), have provided reasonably reliable and faster methods for two-dimensional estimation of the nodule deposits. Owing to differential burial of nodules under the top sediment layers, this study shows how distinct empirical formulae can be developed for estimating nodule abundances from photographs in different areas depending upon the local seafloor features and nodule distribution characteristics. Such data when combined with ground truth and sounding data (Jaishankar and Sharma, 2005; Shippek, 2009) can provide multi-disciplinary environmental information associated with nodules required for planning the mining operations for these deep-sea minerals.

Acknowledgement

We thank the Director, National Institute of Oceanography, Goa for permission to publish this work. This study was carried out during the EIA studies for nodule mining in CIOB funded by the Ministry of Ocean and Earth Sciences, New Delhi. The bathymetry and block-wise nodule data are from PMN data bank. Authors would like to thank Ms. MBL Mascarenhas-Pereira for her help in data processing.

References

- BLUHM, H., 2001 Re-establishment of an abyssal megabenthic community after experimental physical disturbance of the seafloor. *Deep-Sea Research II*, **48**, pp.3841-3868.
- CHAKRABORTY, B., PATHAK, D., SUDHAKAR, M. and RAJU, Y.S., 1996, Determination of nodule coverage parameters using multibeam normal incidence echo characteristics: A study in the Indian Ocean. *Marine Georesources and Geotechnology*, **15**, pp.33-48.
- CRONAN, D. S., 1980, *Underwater minerals*. p362, (London :Academic).
- CRONAN, D. S., 2000, *Handbook of marine mineral deposits*. p406, (Boca Raton:CRC).
- DEMOUSTIER, C., 1985, Inference of manganese nodule coverage from sea beam acoustic backscattering data. *Geophysics*, **50(6)**, pp.989-1001.
- EDWARD, B.D., DARNTTELL, P. and CHEZAR, H., 2003, Characterisation of benthic substrates of Santa Monica Bay with seafloor photography and multibeam sonar imagery. *Marine Environmental Research*, **56**, pp. 47-66.
- FELIX, D., 1980, Some problems in making nodule abundance estimates from seafloor photographs. *Marine Mining*, **2**, pp.293-302.
- FEWKES, R.H., MCFARLAND, W.D., REINHART, W.R. and SORAM, R.K., 1979, Development of a reliable method for evaluation of deep sea manganese nodule deposits. *Bureau of Mines Open File Report 64-80*, US Department of the Interior Bureau of Mines, pp. 91.

- FRAZER, J.Z., FISK, M.B., ELLIOTT, J., WHITE, M. and WILSON, L., 1978, Availability of copper, nickel, cobalt and manganese from ocean ferromanganese nodules. *Annual Report*, June 30, 1977-August 31, 1978, US Department of Commerce, SIO Reference 78-25, pp.105-138.
- FRAZER, J.Z. and FISK, M.B., 1981, Geological factors related to characteristics of sea-floor manganese nodule deposits. *Deep-Sea Research*, **28A (12)**, pp.1533-1551.
- GLASBY, G.P., 1976, Surface densities of manganese nodules in the southern sector of the South Pacific. *N.Z. Journal of Geology and Geophysics*, **19**, pp.771-790.
- HANDA, K. and TSURUSAKI, K., 1981, Manganese nodules: Relationship between coverage and abundance in the northern part of Central Pacific Basin. *Geological Survey of Japan*, **15**, pp.184-217.
- HORN, D. R., HORN, B. M. and DELACH, M. N., 1973, Factors which control the distribution of ferromanganese nodules and proposed research vessel's track, North Pacific. Technical report No 8, NSF-GX33616, Washington D.C., p19.
- IYER, S.D. and SHARMA, R., 1990, Correlation between occurrence of manganese nodules and rocks in a part of the Central Indian Ocean Basin. *Marine Geology*, **92**, pp.127-138.
- IYER, S.D. and SUDHAKAR, M., 1993, Coexistence of pumice and manganese nodule fields-evidence for submarine silicic volcanism in the Central Indian Basin. *Deep-Sea Res.*, **40(5)**, pp.1123-1129.
- JAISANKAR, S. and SHARMA, R., 2005, An interactive end-user software application for a deep-sea photographic database. *Computers and Geosciences*, **31(6)**, pp.718-734.
- JUNG, H., KO, Y., CHI, S. and MOON, J., 2001, Characteristics of seafloor morphology and ferromanganese nodule occurrence in the Korea deep-sea environmental study (KODES) area, NE Equatorial Pacific. *Marine Georesources and Geotechnology*, **19**, pp.167-180.
- KHADGE, N. H., 2005, Changes in geotechnical properties of sediments from the Central Indian Basin induced by disturbance experiment. *Marine Georesources and Geotechnoogy*, **23(4)**, pp.401-417.
- KUNZENDORF, H., 1986, *Marine Mineral Exploration*. p300, (Amsterdam: Elsevier).
- LENOBLE, J.P., 1980 Technical problems in ocean mining evaluation. In *Geology and geochemistry of manganese*, Varentsev, I.M., and Grasselly, G.J. (Eds.), pp.327-342 (Budapest: Hungarian academy of sciences).
- MERO, J. L., 1962, Ocean floor manages nodules, *Economic Geology*, **57**, 747-767.
- MUKHOPADHYAY, R. and NATH, B. N., 1988, Influence of seamount topography on the local facies variation in ferromanganese deposits in the Indian Ocean. *Deep-Sea Res.*, **35**, pp.1431-1436.
- PARK, S.H., KIM, D.H., KIM, C., PARK, C.Y. and KANG, J.K., 1997, Estimation of coverage and size distribution of manganese nodules based on image processing techniques. *Proceedings of the Second Ocean Mining Symposium*, Seoul, Korea, November, 24-26, pp.40-44.

- PATTAN, J.N. and PARTHIBAN, G., 2007, Do manganese nodules grow or dissolve after burial? Results from the Central Indian Ocean Basin. *Journal of Asian Earth Sciences*, **30**, pp.696-705.
- RODRIGUES, N., SHARMA, R. and NATH, B.N., 2001, Impact of benthic disturbance on megafauna in Central Indian Basin. *Deep-Sea Research II*, **48**, pp.3411-3426.
- SHARMA, R., 1989, Effect of sediment-water interface 'Boundary Layer' on exposure of nodules and their abundance: a study from seabed photos. *Journal of Geological Society of India*, **34**, pp.310-317.
- SHARMA, R. and RAO, A.S., 1992, Geological factors associated with megabenthic activity in the Central Indian Basin. *Deep-Sea Research*, **39(3/4)**, pp.705-713.
- SHARMA, R., 1993, Quantitative estimation of seafloor features from photographs and their application to nodule mining. *Marine Georesources and Geotechnology*, **11(4)**, pp.311-331.
- SHARMA, R., and KOAGALI, V. N., 1993, Influence of seabed topography on the distribution of manganese nodules and associated features in the Central Indian Basin: A study based on photographic observations. *Marine Geology*, **110(1-2)**, pp.153-162.
- SHARMA, R., 1998, Nodule distribution characteristics and associated seafloor features: Factors for exploitation of deep-sea Fe-Mn deposits. *Society for Mining, Metallurgy and Exploration INC.*, **304**, pp.16-22.
- SHARMA, R., JAISANKAR, S., SAMANTA, S., SARDAR, A.A. and GRACIOUS, D., 2010, Image analysis of seafloor photographs for estimation of deep-sea minerals. *Geo-Marine Letters*, **30(6)**, pp. 617-626.
- SHIPEK, C.J., 2009, Photographic study of some deep-sea floor environments of the Eastern Pacific. *Geological Society of America Bulletin*, **71**, pp.1067-1074.
- UNOET, 1982, Reliability of the Data Parameters. In *Assessment of manganese nodule resources. Seabed minerals: Vol. 1*, pp. 15-27 (London: United Nations Ocean Economics and Technology Branch, Graham and Tretman).
- VALSANGKAR, A.B. and KHADGE N. H., 1989, Size analyses and geochemistry of ferromanganese nodules from the Central Indian Ocean Basin. *Marine Mining*, **8(3)**, pp.325-347.
- VINEESH, T.C., NATH, B.N., BANERJEE, R., JAISANKAR, S. and LEKSHMI, V., 2009, Manganese nodule morphology as indicators for oceanic processes in the Central Indian Basin. *International Geology Review*, **51**, pp.27-44.
- YAMAZAKI, T. and SHARMA, R., 2000, Morphological features of Co-rich manganese deposits and their relation to seabed slopes. *Marine Georesources and Geotechnology*, **18**, pp.43-76.

Table 1: Distribution of nodules and associated features from photography data

Features / data	Water Depth (m)	Nodule coverage (%)	Crust coverage (%)	Sediment coverage (%)	Seabed slope (degree)
Minimum	4975	0	0	0	0
25% tile	5236	0	0	95	0
Median	5184	0	0	100	0
75% tile	5178	5	0	100	5
Maximum	5433	79	89	100	76
Mean	5205	8.95	0.28	89.60	2
Std. Dev.	79.67	18.06	13.05	20.70	3.69

Table 2: Physical properties of sediments at two stations

Station No.	Shear Strength (kPa)	Water Content (% dry basis)	Wet density (g/cm³)	Porosity (%)
SVBC20	4.21	491	1.13	91.1
SVBC25	4.31	532	1.12	91.6

Table 3: Thickness of ATL and nodule abundance

Station No.	Thickness of ATL (m)	Abundance (kg/m²)
SVBC-26	31	0.76
SVBC-25R	60	0
SVBC-28	29	2.88
SVBC-27	37	0.04
SVBC-03	17	4.4
SVBC-20	10	0.04
SVBC-31	44	0
SVBC-29	41	1.36
SVBC-30	32	0
SVBC-32	17	10.2
SVBC-04	19	10.68
SVBC-19	20	8.24
SVBC-33	54	0.4
SVBC-18	46	0.88
SVBC-34R	8	3.68
SVBC-35	20	10.72
SVBC-13	15	3.12
SVBC-37	25	0.48
SVBC-36	22	8.88
SVBC-38	12	0.8

Table 4: Details of photo and grab data along deep-tow profiles

Sr. No.	Profile No.	Photo No.	Photo location		Water Depth (m)	Nodule Coverage (%)	Grab location		Nodule Abundance (kg/m ²)
			Latitude (°S)	Longitude (°E)			Latitude (°S)	Longitude (°E)	
1	9-1	626	12.941	74.782	5184	00	12.936	74.782	2.80
2	9-1	1110	12.999	74.855	5184	00	12.996	74.869	1.93
3	9-1	2187	13.130	75.031	5184	55	13.130	74.992	10.81
4	9-1	2433	13.168	75.076	5184	56	13.167	75.086	17.20
5	9-1	473	13.324	75.242	5184	00	13.253	75.244	5.10
6	12-1	1465	12.479	74.943	5109	26	12.508	74.961	9.05
7	12-1	1626	12.504	74.965	5152	00	12.504	74.966	1.20
8	12-1	2589	12.642	75.080	5104	05	12.647	75.064	6.40
9	12-2	824	12.878	75.276	5198	00	12.878	75.241	1.77
10	12-2	1161	12.932	75.322	5219	00	12.932	75.320	0.00
11	12-2	1628	13.013	75.384	5191	34	13.018	75.385	13.85
12	12-2	2496	13.147	75.500	5131	26	13.149	75.503	8.00
13	4-4	129	12.700	75.652	5301	00	12.700	75.650	6.00
14	4-4	718	12.780	75.726	5071	48	12.779	75.735	9.20
	Total					250			93.31

Table 5: Estimation of nodule abundance using different C factors for different nodule coverage (for nodule diameter = 2 cm)

Nodule coverage (%)	Abundance (kg/m ²) estimated with	
	C factor = 18.72	C factor = 14.90
10	3.744	2.98
20	7.488	5.96
30	11.232	8.94
40	14.976	11.92
50	18.72	14.9
60	22.464	17.88
70	26.208	20.86
80	29.952	23.84
90	33.696	26.82
100	37.440	29.8

Captions to Figures

Fig. 1: Nodules with associated seafloor features (a) Photo no. 12-1-1: 10279, area: 4.29x2.86m, with nodules (65% coverage); (b) Photo no. 12-1-1: 10260, area:5.34x3.56m, with nodules (23% coverage) and crust (32% coverage).

Fig. 2: Location of site and survey tracks in Central Indian Ocean Basin

Fig. 3: Bathymetry map of the study area (contours and scale indicate depth in meters)

Fig. 4: Nodule distribution in the study area (contour and scale indicate coverage in %)

Fig. 5: Crust distribution in the study area (contours and scale indicate coverage in %)

Fig. 6: Sediment distribution in the study area (contours and scale indicate coverage in %)

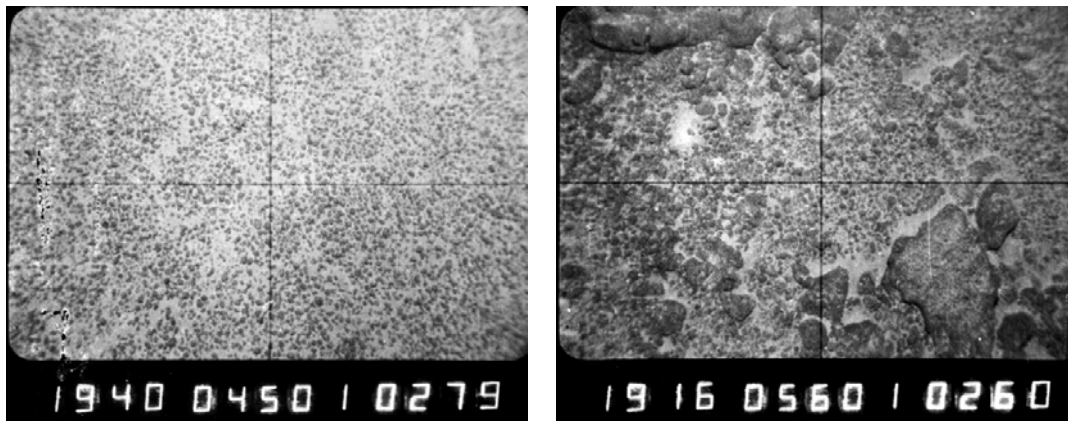
Fig. 7: Seabed slopes in the study area (contours and scale indicate slope in degrees)

Fig. 8: Estimation of mean nodule abundance (kg m^{-2}) in the study area Fig. 9: ATL thickness from Parasound data in study area: (a) $\sim 10\text{m}$, and (b) $\sim 60\text{m}$

Fig. 9: ATL thickness from Parasound data in study area: (a) thickness $\sim 10\text{m}$, (b) thickness $\sim 60\text{m}$

Fig. 10: Distribution of depth and ATL thickness in different topographic domains

Fig. 11: Relationship of ATL thickness with nodule abundance



(a)

(b)

Fig. 1: Nodules with associated seafloor features (a) Photo no. 12-1-1: 10279, area : 4.29x2.86m, with nodules (65% coverage); (b) Photo no. 12-1-1: 10260, area : 5.34x3.56m, with nodules (23% coverage) and crust (32% coverage).

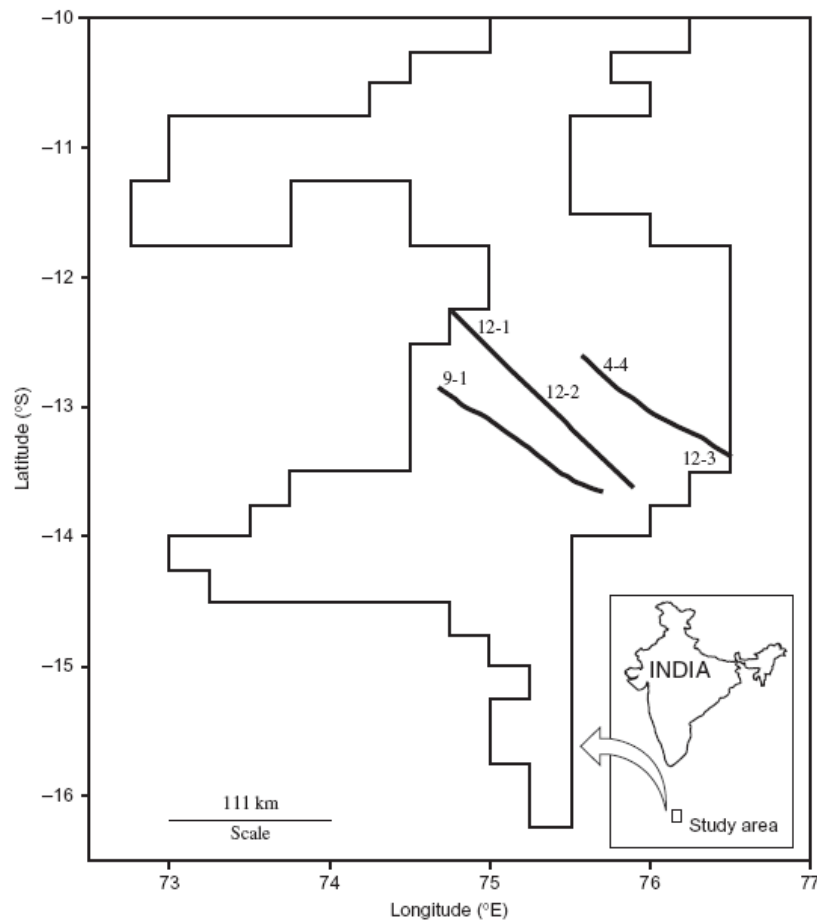


Fig. 2: Location of site and survey tracks in Central Indian Ocean Basin

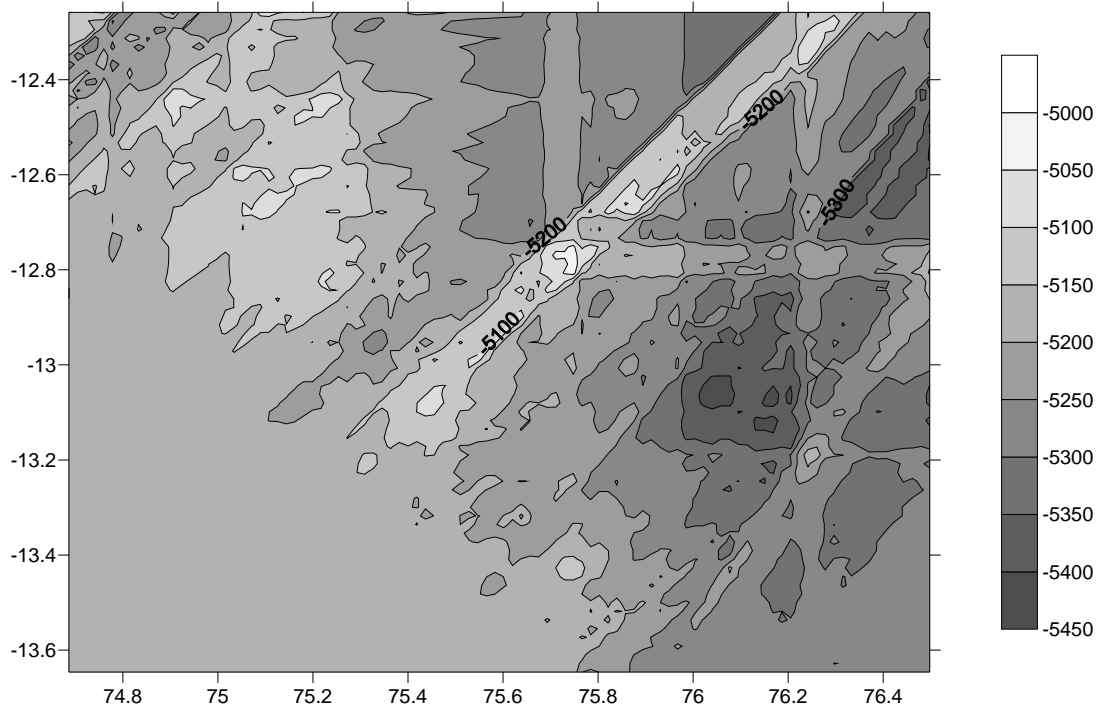


Fig. 3: Bathymetry map of the study area (x-axis is longitudes in °E, y-axis is latitudes in °S, contours and scale indicate depth in meters)

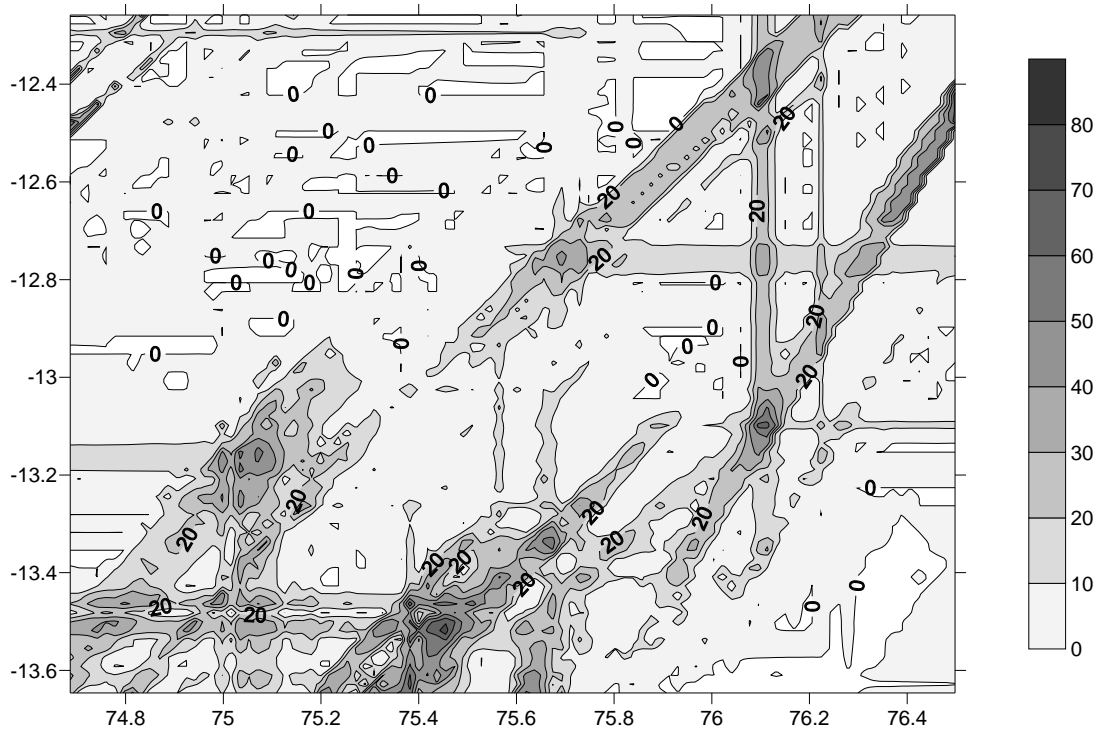


Fig. 4: Nodule distribution in the study area (x-axis is longitudes in °E, y-axis is latitudes in °S, contours and scale indicate coverage in %)

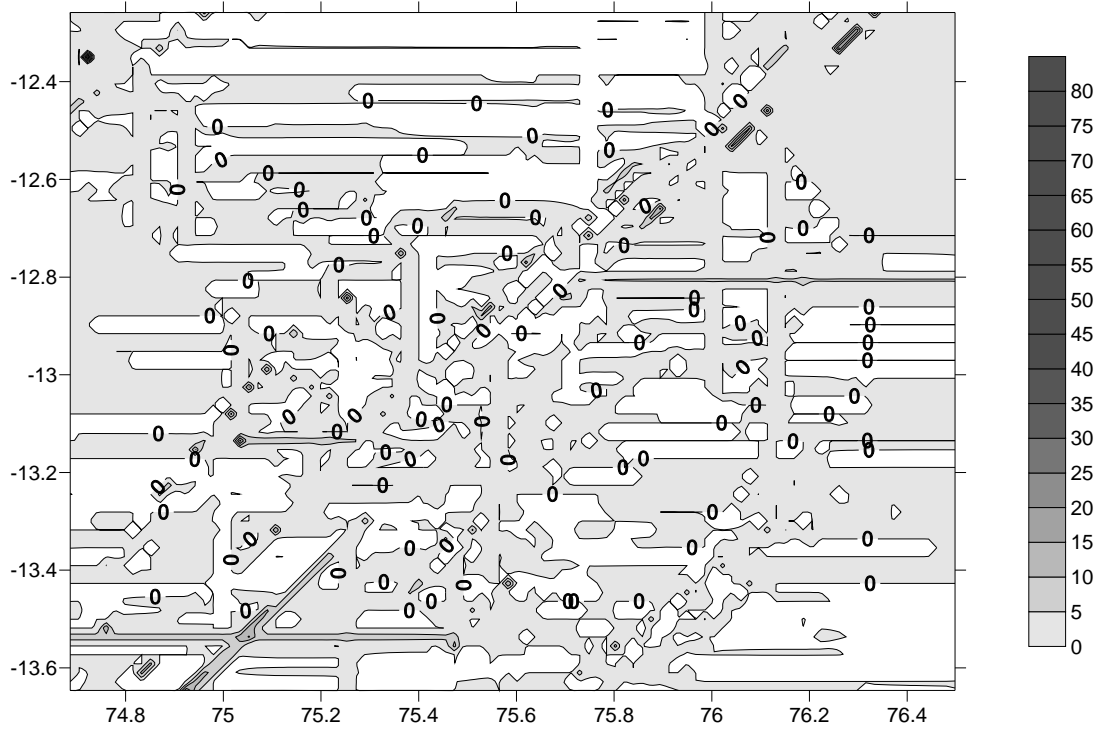


Fig. 5: Crust distribution in the study area (x-axis is longitudes in °E, y-axis is latitudes in °S, contours and scale indicate coverage in %)

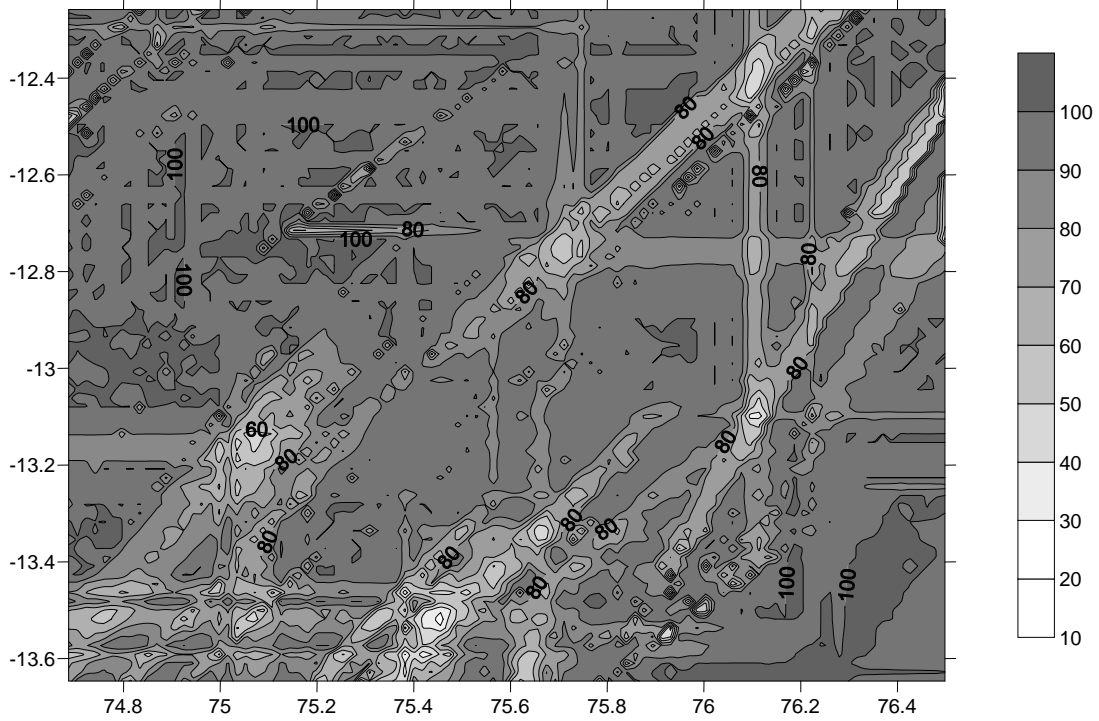


Fig. 6: Sediment distribution in the study area (x-axis is longitudes in °E, y-axis is latitudes in °S, contours and scale indicate coverage in %)

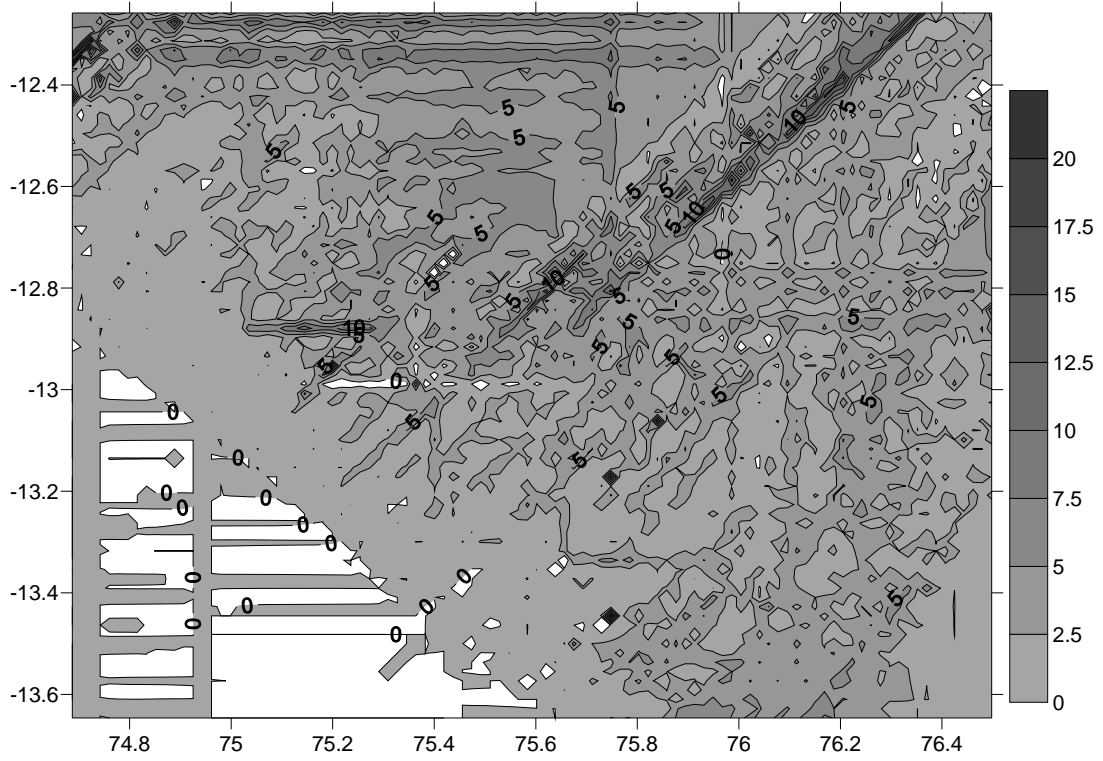


Fig. 7: Seabed slopes in the study area (x-axis is longitudes in °E, y-axis is latitudes in °S, contours and scale indicate slope in degrees)

	74.5 E	75.0 E	75.5 E	76.0 E	76.5 E
12.0 S	N = 2 Max = 9.05 Min = 0.68 Total = 9.73 Mean= 4.86	N = 22 Max = 10.44 Min = 0.43 Total = 84.50 Mean= 3.84	N = 40 Max = 43.60 Min = 0.77 Total = 221.64 Mean= 5.54	N = 33 Max = 13.32 Min = 0.00 Total = 173.92 Mean= 5.27	
12.5 S	N = 14 Max = 19.61 Min = 0.62 Total = 90.25 Mean = 6.45	N = 27 Max = 11.99 Min = 0.57 Total = 127.80 Mean= 4.73	N = 21 Max = 22.00 Min = 0.77 Total = 166.60 Mean = 7.93	N = 0 Max = - Min = - Total = - Mean = -	
13.0 S	N = 6 Max = 14.65 Min = 1.21 Total = 42.68 Mean= 7.11	N = 17 Max = 17.20 Min = 0.55 Total = 140.89 Mean= 8.23	N = 4 Max = 14.77 Min = 3.46 Total = 30.15 Mean= 7.54	N = 0 Max = - Min = - Total = - Mean = -	
13.5 S					

Fig. 8: Estimation of mean nodule abundance (kg m^{-2}) in the study area

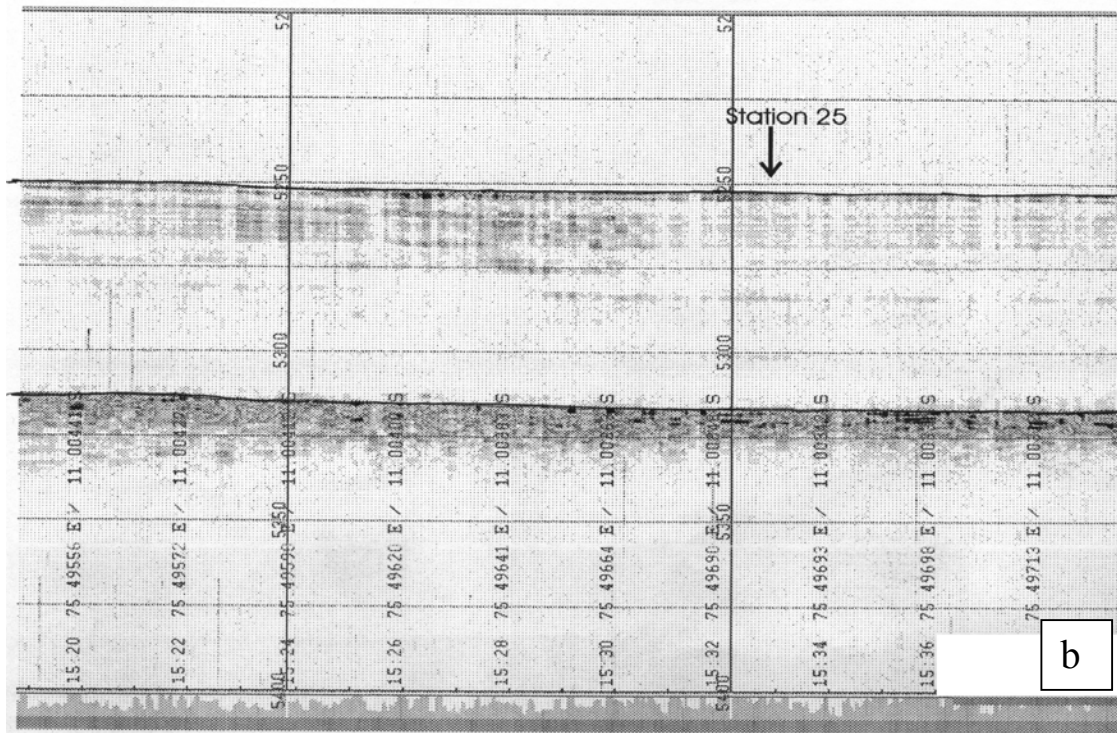
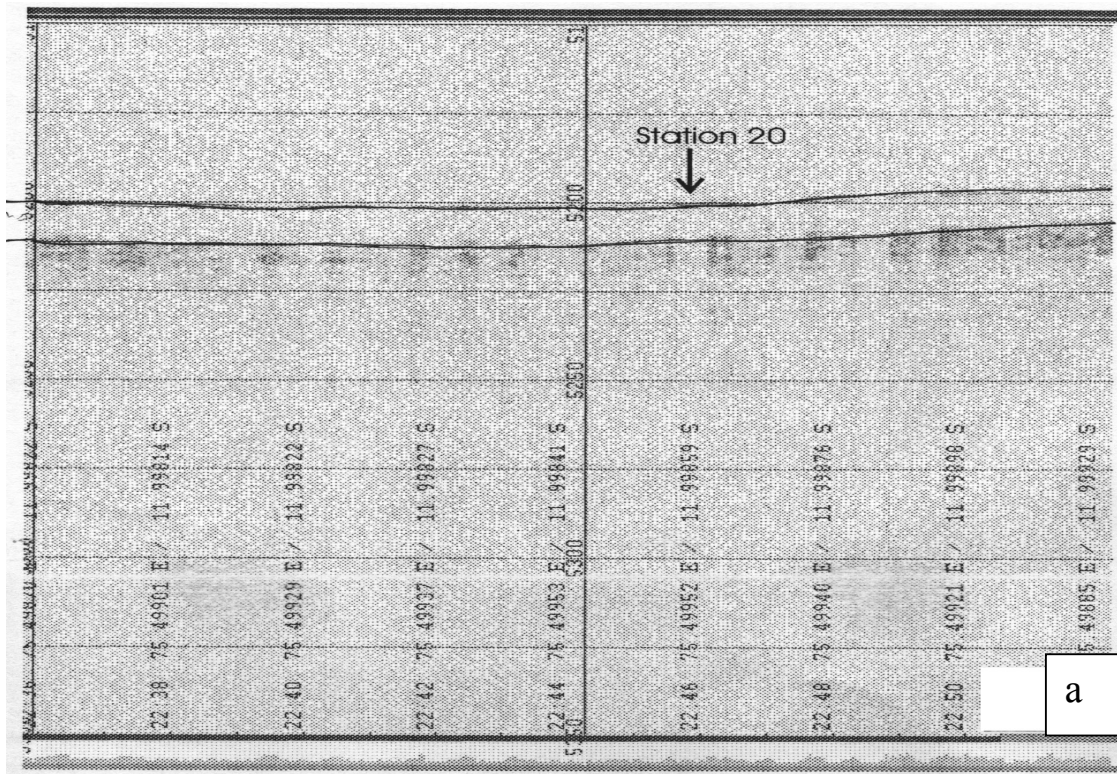
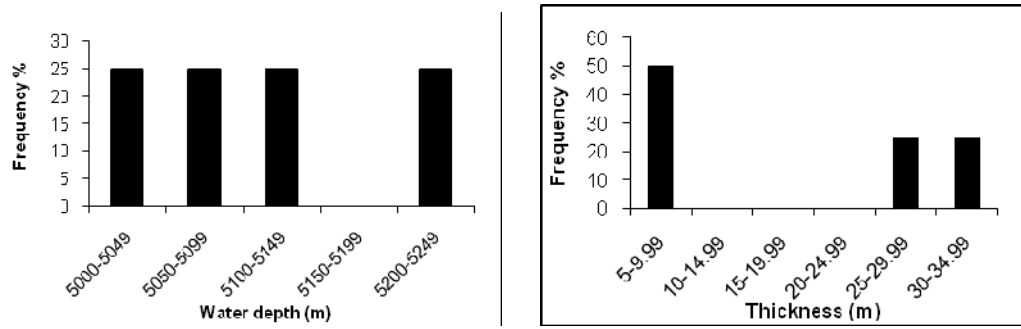
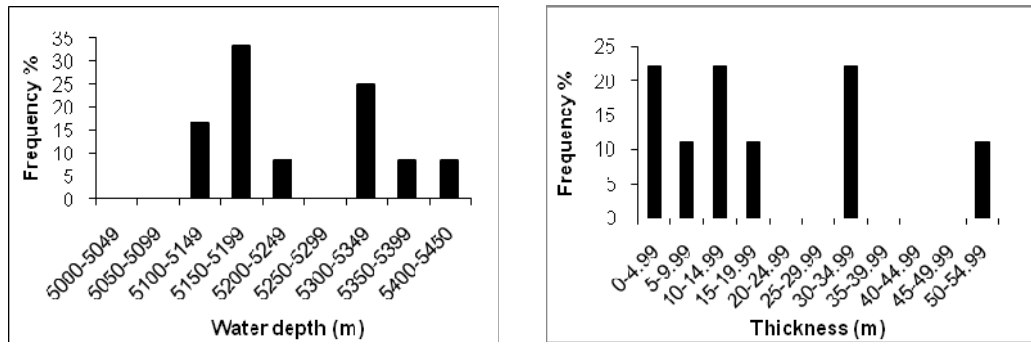


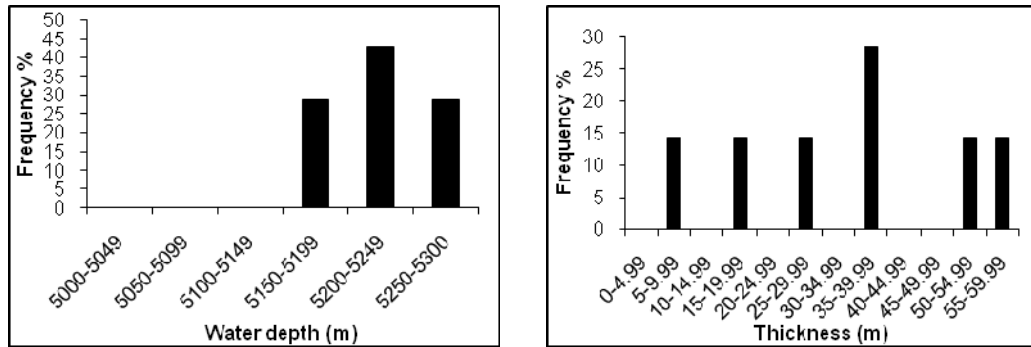
Fig. 9: ATL thickness from Parasound data in the study area: (a) thickness ~ 10m, (b) thickness ~ 60m



(a) Hilltops



(b) Slopes



(c) Valleys

Fig. 10: Distribution of depth and ATL thickness in different topographic domains

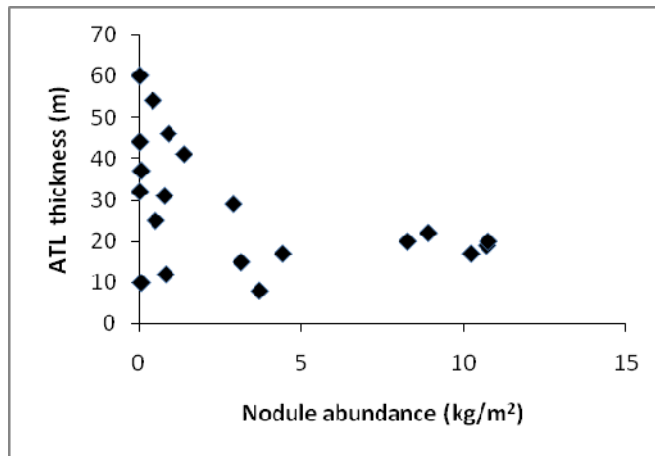


Fig. 11: Relationship of ATL thickness with nodule abundance